Journal of Alloys and Compounds, 183 (1992) 7–17
JALCOM 7002

Crystal structure and electronic structure of $Nb_xTa_{2-x}S$ ($x \approx 0.95$): a new layered compound in ternary Ta–Nb–S system*

Xiaoqiang Yao, Gordon J. Miller and Hugo F. Franzen
Department of Chemistry, Iowa State University, Ames, IA 50011 (USA)

Abstract

During the continuing study of the metal-rich region of the ternary Ta–Nb–S system a new layered compound, $Nb_xTa_{2-x}S$ ($x \approx 0.95$), was found using the arc-melting method and characterized by means of X-ray diffraction experiments. The compound crystallizes in the tetragonal space group *P4/nmm* with unit cell dimensions $a = 333.04(7)$ pm and $c = 909.28(94)$ pm. The tetragonal cell contains two formula units. The structure contains homoatomic layers sequenced S–M2–M1–M1–M2–S (M is a Nb, Ta mixture) generating six-layer sheets stacked along [001] and is closely related to b.c.c. Weak S–S interactions at 319 pm between sheets contrast with the M–M binding within and between the sheets, the former presumably being responsible for the observed graphitic slippage of the samples. Based upon extended Hückel band calculations metallic properties can be expected for this compound. The relative preference of the metal sites for the two metal elements (Ta, Nb) is explained by band calculations.

1. Introduction

In recent years, a variety of substitutional ternary metal-rich chalcogenides, *i.e.* compounds in which some or all of the metal positions are occupied by two kinds of metals, have been found. These chalcogenides can be divided into two categories: the first includes the compounds which are isostructural with known binary metal-rich compounds, *e.g.* $Hf_xTi_{21-x}S_8$ ($x = 7.47$) [1] ($Nb_{21}S_8$ [2] type), $M_xNb_6S_{3-x}$ (M≡Fe, Co and Ni; $x \approx 1$) [3] and $Cu_xNb_6S_{3-x}$ ($x = 0.46$) [4] (Ta_2P [5] type), and $V_xNb_{14-x}S_5$ ($x = 3.14$) [6] ($Nb_{14}S_5$ [7] type); the second includes the compounds which exhibit new structure types, *e.g.* $M_xTa_{6-x}S$ (M≡V and Cr, $x \approx 1$) [8] and $Nb_9Ni_{2-x}S_{3+x}$ ($x = 0.63$) [3].

We are currently exploring solid-state chemistry in the ternary Ta–Nb–S system. As well as some compounds, *e.g.* $Nb_{21-x}Ta_xS_8$ ($x = 6.2$) [9] ($Nb_{21}S_8$ [2] type) exhibiting substitutional solid solution, three new compounds, $Nb_xTa_{4-x}S_{11}$ ($x = 4.92$) [10], $Nb_{12-x}Ta_xS_4$ ($x = 5.26$) [11] and $Nb_xTa_{5-x}S_2$ ($x = 1.72$) [12] exhibiting new structure types have been found. The structures of the first two compounds, $Nb_xTa_{11-x}S_4$ and $Nb_{12-x}Ta_xS_4$ have features that

*Dedicated to Professor W. Bronger and Professor Ch. J. Raub on the occasions of their 60th birthdays.

0925-8388/92/$5.00

are reminiscent of the Nb-rich sulfides, $Nb_{21}S_8$ [2] and $Nb_{14}S_5$ [7]. $Nb_xTa_{5-x}S_2$ ($x=1.72$) [12] is a new layered compound in which there are van der Waals gaps separated by a robustly metallic region. A new layered compound, $Nb_xTa_{2-x}S$ ($x\approx0.95$, $P4/nmm$, $a=333.04(7)$ pm and $c=909.28(94)$ pm) isostructural with Ta_2Se [13], was found during this continuing investigation.

2. Experimental details

2.1. Sample preparation

High purity niobium (Alpha Products, Danvers, MA) and sulphur (Fisher Scientific Co., Fair Lawn, NJ) were put into a previously degassed silica tube in the molar ratio: $n_{Nb}:n_S=2:1$ and were heated at 1000 K for 5 days in a tube furnace. TaS was synthesized using a similar method. The mixture of "Nb_2S" (there is no known compound with the formula Nb_2S), TaS and Ta ($n_{Ta}:n_{Nb}:n_S=3:2:2.17$) was pressed into a pellet and arc-melted three times on a water-cooled copper plate using a thoriated nonconsumable tungsten electrode in an argon atmosphere. The Guinier X-ray powder pattern (Vacuum Guinier camera FR552, Enraf Nonius, Delft, The Netherlands) using Cu $K\alpha_1$ and silicon as an internal standard indicated that a new phase existed together with elemental Ta and less than 2% NbS [14] in the sample. However, the powder pattern of the arc-melted sample was diffuse, which indicated that the sample was not well crystallized (if the sample was arc-melted for longer, $Nb_xTa_{5-x}S_2$ [12] was also found in the sample). An attempt was made to anneal the arc-melted sample. The sample was annealed for 10 h in an induction furnace at 1700 K; during which the new phase disappeared, and $Nb_xTa_{11-x}S_4$ [10] and unknown phases were formed. The arc-melted sample was then placed in a degassed silica tube and annealed for 5 weeks at a lower temperature (1100 K) in a tube furnace.

2.2. Single-crystal X-ray investigation

A large number of crystals were found in the annealed sample. A gray-colored crystal ($0.03\times0.04\times0.15$ mm^3) was picked from the annealed sample and attached to a glass fiber using apiezon grease (the crystal was deformed when epoxy glue was used). Intensity data were collected using monochromatic Mo $K\alpha$ radiation, employing the 2θ–ω scan technique up to 65° (2θ) on a Rigaku AFC6 single-crystal diffractometer. A total of 763 reflections (hkl, $-hkl$, $-hk-l$, $-hk-l$) were monitored, and 104 unique reflections with $F^2>3\sigma(F_0^2)$ were obtained and used for the structure determination. The observed intensities were corrected for Lorentz polarization and absorption effects with an empirical absorption coefficient of 622.93 cm^{-1}. Based on three standard reflections measured every 150 reflections, there was no significant fluctuation or decay of the crystal. Subsequent data processing and structure calculations were performed with the TEXSAN program package.

The space group was determined to be $P4/nmm$ using the PROCESS program. First, an empirical absorption correction was applied with the

maximum and minimum transmission factors of 1.000 and 0.301 respectively. The application of direct methods resulted in an electron map containing three strong peaks per asymmetric unit on the x, $y = 1/4$ sections. Two of these peaks were much higher than the third one. The two stronger peaks were taken to be at Ta positions and the third peak to be at an S position; and the refinement was initiated. The multiplicities for the metal positions were refined after 50% Ta and 50% Nb was assigned on each metal position. Finally, the isotropic thermal parameters were refined with the concomitant refinement of the multiplicities for the metal positions, and the R, R_w and goodness of fit indicator (GOF) values were obtained as 0.048, 0.046 and 1.647 respectively. The composition was obtained as $Nb_{0.59}Ta_{1.41}S$ from the isotropic refinement (because the secondary extinction coefficient became negative when refined, it is concluded that there is no significant secondary extinction in the compound).

After isotropic refinement, F_c values for $Nb_{0.59}Ta_{1.41}S$ were calculated and used for a DIFABS [15] absorption correction for the F_0 values in the mode that utilizes θ-dependent systematic deviations $|F_0| - |F_c|$. The ratio of the highest to the lowest transmission was 1.385. The anisotropic thermal parameters were refined with the concomitant refinement of the multiplicities for the metal positions and the final R, R_w and GOF values were obtained as 0.048 and 0.048 and 1.054 respectively. The composition was determined to be $Nb_{0.95}Ta_{1.05}S$ from the anisotropic refinement. (The R, R_w and GOF values were obtained as 0.048, 0.049 and 1.069 respectively, if the multiplicities for the metal positions were fixed (*i.e.* the composition was $Nb_{0.59}Ta_{1.41}S$ during the anisotropic refinement). However, the first approach appears to be more reasonable. There are two impurity peaks higher than $5e^-$ $Å^{-3}$ (5.695 and 5.267 e^- $Å^{-3}$) in the second approach results compared with only one impurity peak higher than $5e^-$ $Å^{-3}$ (5.291 e^- $Å^{-1}$) in the approach results. In addition, the ratio U_{33}/U_{11} for the sulfur atom was approximately ten in the second approach, compared with approximately three in the first approach. The trend that Nb preferentially occupies the metal positions bound to more S is true for the results of both approaches. Based on the above arguments, we prefer the result of the first approach. The crystal data, atom parameters, bond distances and powder diffraction data are given in Tables 1, 2, 3 and 4 respectively.

Figures 1 and 2 show representations of $Nb_xTa_{2-x}S$ ($x \approx 0.95$). A list of observed and calculated structure factors is available upon request from the authors.

3. Results and discussion

3.1. The structure of $Nb_xTa_{2-x}S$

$Nb_xTa_{2-x}S$ is isostructural with Ta_2Se [13]. In the structure of $Nb_xTa_{2-x}S$, each metal position is fractionally occupied by Nb and Ta and the metal positions have been labeled so that as the metal indicator increases, the

TABLE 1

Crystal data for $Nb_{0.95}Ta_{1.05}S$

Formula	$Nb_{0.95}Ta_{1.05}S$
Formula weight	310.32
Space group	$P4/nmm$(No. 129)
a (Å)	3.3304(7)[a]
c (Å)	9.0928(94)[a]
V (Å^3)	100.85(11)[a]
Z	2
d_{calc} (g cm^{-3})	10.275
Crystal size, (mm^3)	0.03×0.04×0.15
μ(Mo Kα) (cm^{-1})	622.93
Data collection instrument	Rigaku AFC6R
Radiation (monochromated in incident beam)	Mo Kα (λ=0.71069 Å)
Orientation reflections, number, range (2θ)	23, 14–40
Temperature (°C)	22
Scan method	2θ–ω
Octants measured	$hkl, -hkl, hk-l, -hk-l$
Data collection range, 2θ (deg)	0–65
No. reflections measured	763
No. unique data, total with $F_0^2 > 3\sigma(F_0^2)$	104
No. parameters refined	12
Transmission factors, (maximum, minimum)	1.000, 0.301
$R_{av.}$	0.14
R[b]	0.048
R_w[c]	0.048
Largest shift/e.s.d., final cycle	0.00
Largest peak, (2e$^-$ Å^{-3})	5.29

[a]Obtained from indexing of the powder pattern.
[b]$R = (\Sigma \| |F_o| - |F_c| \|)/(\Sigma |F_o|)$
[c]$R_w = [\Sigma w(|F_o| - |F_c|)^2/\Sigma w|F_o|^2]^{1/2}$; $w = 1/\sigma^2(|F_o|)$

TABLE 2

Atomic coordinates for $Nb_{0.95}Ta_{1.05}S$[a]

Atom	Site	Occupancy (%)	z	B_{eq}	U_{11}	U_{33}
M1	2c	76.6Ta+23.4Nb	0.4146(1)	0.22(3)	0.0031(6)	0.0020(6)
M2	2c	28.2Ta+71.8Nb	0.7761(2)	0.37(5)	0.0041(7)	0.006(1)
S	2c		0.119(1)	0.6(2)	0.005(2)	0.014(4)

[a]$x, y = 1/4$ for all atoms, $U_{22} = U_{11}$, $U_{ij} = 0$. $B_{eq} = 8\pi^2/3(U_{11} + U_{22} + U_{33})$

n_{Nb}/n_{Ta} ratio on that position also increases, *i.e.* from M1 to M2 the n_{Nb}/n_{Ta} on the metal position increases. Figure 1 is a projection of the structure onto the xz plane (the unit cell is marked using solid lines). The structure of $Nb_xTa_{2-x}S$ is similar to that of $Nb_xTa_{5-x}S_2$ [12] in that the structure can

TABLE 3

Bond distances (pm) in $Nb_{0.95}Ta_{1.05}S$ (<340 pm)

Atom	Neighbor	Distance (pm)
M1	M1	4×333.04(7)
	M1	4×282.1(2)
	M2	4×292.5(2)
	M2	328.7(4)
	S	269(1)
M2	M1	4×292.5(2)
	M1	328.7(4)
	M2	4×333.04(7)
	S	4×254.1(4)
	S	312(1)
S	M1	269(1)
	M2	4×254.1(4)
	M2	312(1)
	S	4×320(1)
	S	4×333.04(7)

TABLE 4

X-ray powder diffraction of $Nb_{0.95}Ta_{1.05}S$ (Cu $K\alpha_1$ radiation)[a] ($2\theta < 75°$)

$h\ k\ l$	$2\theta_{obs}$	$2\theta_{calc}$	I_{obs}[b]	I_{calc}
0 0 1	9.63	9.72	s	71.9
1 0 2	33.35	33.32	s	40.8
1 1 0	38.21	38.18	s	66.1
1 1 1	39.46	39.49	w	11.1
1 0 3	40.19	40.19	s	100.0
0 0 5		50.12		6.9
2 0 0	55.10	55.10	m	24.9
0 0 6		61.10		5.5
1 1 5	64.68	64.71	w	14.9
2 1 2	65.95	65.94	w	15.1
2 1 3	70.34	70.37	m	49.7
1 1 6	74.32	74.37	w	14.7

[a] 2θ values of reflections with relative intensities $I_{calc} > 5$ are listed.
[b] w, weak; m, medium; s, strong.

be viewed as a b.c.c.-type Nb–Ta solid solution in which two neighboring layers in every six (compared with every seven in $Nb_xTa_{5-x}S_2$) are replaced by S. Some distortions relative to b.c.c.-type structure are observed, *e.g.* there is a contraction of the cube consisting of four M1 and four M2 along the *c* axis with M1 deviating slightly from the center of the cube. The coordinations around each atom may be thought of, approximately, as capped distorted cubes. The M1 atom is surrounded by 14 atoms: four M1 atoms (282.1 pm distant) and four M2 atoms (292.5 pm distant) at the corners

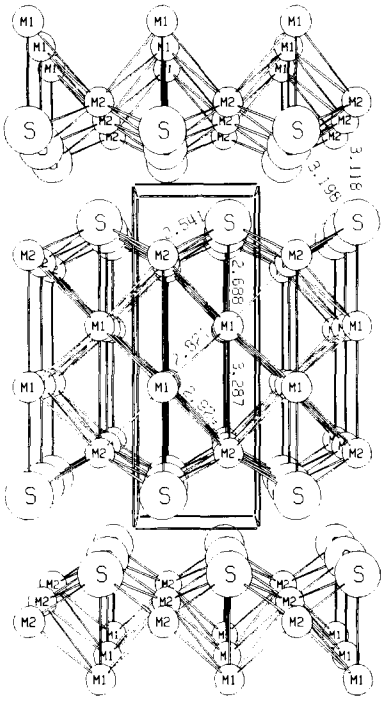

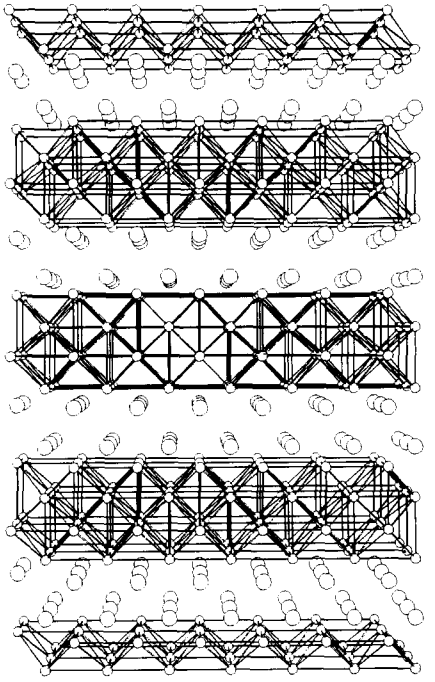

Fig. 1. The projection of $Nb_xTa_{2-x}S$ ($x \approx 0.95$) on the xz plane. The vertical is the z direction. The unit cell is marked by solid lines.

Fig. 2. The projection of $Nb_xTa_{2-x}S$ ($x \approx 0.95$) on the xz plane. The vertical is the z direction. The larger circles represent S.

of a distorted cube; four M1 atoms (333.04 pm distant), one M2 atom (328.7 pm distant) and one S atom (269 pm distant) as capping atoms. For M2, the surrounding atoms are as follows: four M1 atoms (292.5 pm, distant) and four S atoms (254.1 pm distant) at the corners of a distorted cube; one M1 atom (328.7 pm distant), four M2 atoms (333.04 pm distant) and one S atom (312 pm distant) as the capping atoms. The corners of the distorted cube around the S atom are four M2 atoms (254.1 pm distant) and four S atoms (320 pm distant) with one M1 atom (269 pm distant), one M2 atom (312 pm distant) and four S atoms (333.04 pm distant) as the capping atoms. The shortest distance between two sulfur atoms in two neighboring layers is 320 pm, and apparently the S–4M–S sandwiches are held together by van der Waals interactions. These interactions lead to graphitic properties and the observed tendency of the crystal of the compound to be deformed by the drying of epoxy glue.

Because there are one and five coordinating sulfur atoms around the M1 and M2 atom respectively, this is the fifth example (along with $Nb_{21-x}Ta_xS_8$ [9], $Nb_xTa_{11-x}S_4$ [10], $Nb_{12-x}Ta_xS_4$ [11] and $Nb_xTa_{5-x}S_2$ [12]) in which it has been found that the Nb occupation of a site occupied by both Nb and

Ta increases with the number of S atoms in the first coordination sphere of that position.

The compound $Nb_xTa_{2-x}S$ can be obtained with some range of homogeneity. As Nb and Ta have nearly the same radii, the cell constants show negligible change with x. $Nb_xTa_{2-x}S$ can be obtained for $n_{Ta}/n_{Nb} > 1$. The exact range of x in the compound has not been determined.

An attempt was made to synthesize $Nb_{0.95}Ta_{1.05}S$ from a stoichiometrically appropriate mixture of Ta, TaS and "Nb_2S" using the arc-melting method mentioned in Section 2. Two phases, $Nb_xTa_{2-x}S$ and $Nb_{1-x}Ta_xS$ (NbS type [14]), were found to coexist in the product from the X-ray powder diffraction pattern. The ratios of n_{Ta}/n_{Nb} were determined to be 1.29 and 0.81 for $Nb_xTa_{2-x}S$ and $Nb_{1-x}Ta_xS$ respectively, using the energy dispersion analysis by X-rays (EDAX) method in a scanning electron microscope. These values correspond to $Nb_{0.87}Ta_{1.13}S$ ($Nb_xTa_{2-x}S$) and $Nb_{0.55}Ta_{0.45}S$ ($Nb_{1-x}Ta_xS$). This means that samples with $n_{Ta}/n_{Nb} = 1.05/0.95$ (1.11) favor the formation of mixtures of $Nb_xTa_{2-x}S$ and $Nb_{1-x}Ta_xS$ (NbS type), suggesting that the n_{Ta}/n_{Nb} ratio determined by the single crystal refinement is probably slightly lower than the correct value. However, this discrepancy appears unavoidable given the solid-solution character of this high-temperature phase.

3.2. Bonding in $Nb_xTa_{2-x}S$ ($x \approx 0.95$)

Band calculations were carried out for $Nb_xTa_{2-x}S$ using the extended Hückel method. The parameters used for band calculations are given in Table 5. The valence-state ionization energies (H_{ii}s) for Ta and Nb were obtained from a charge-iterative calculation on Nb_5S_2 and Ta_5S_2 in the $Nb_xTa_{5-x}S_2$ structure [12] (S parameters were cited from ref. 16).

Because the band theory cannot deal explicitly with the compounds in which one position is occupied by two kinds of elements, some assumptions were made to enable the calculation. The overall atomic ratio of Ta/Nb is

TABLE 5

Atomic parameters used in the calculations

Atom	Orbital	H_{ii} (eV)	ξ_1[a]	ξ_2[a]	c_1[b]	c_2[b]
Ta	5d	−11.21	4.76	1.94	0.6815	0.6815
	6s	−12.22	2.28			
	6p	−7.97	2.24			
Nb	4d	−11.97	4.08	1.64	0.6401	0.5516
	5s	−10.41	1.89			
	5p	−6.44	1.85			
S	3s	−20.00	1.82			
	3p	−13.30	1.82			
	3d	−8.00	1.50			

[a]Exponent in the double ξ function for d orbitals.
[b]Slater-type orbitals exponents.

observed to be close to 1 and Nb is observed to occupy preferentially the M2 site relative to the M1 site. Thus (the sequence of M1, M2 and S is M1M2S in this formula), the arrangement TaNbS is closer to the real one than is NbTaS.

Figure 3 is a plot of the density of states (DOS) for $Nb_xTa_{2-x}S$ ($x \approx 0.95$). Although there is a local minimum in the DOS at the Fermi level, clearly there is no gap in the DOS around the Fermi level. Thus $Nb_xTa_{2-x}S$ is expected to exhibit metallic properties, *e.g.* metallic electrical conductivity. The values of the overlap population (OP) for each symmetry-unique pair of atoms, the average energy and the values of the charge (valence electron) on each atom position for the two arrangements (TaNbS and NbTaS) are given in Tables 6 and 7 respectively.

The sums of OPs for all metal–metal bonds and for all bonds in the structure for the two arrangements, appropriately weighted to reflect the number of each symmetry-unique bond, are also given in Table 6. The values of summations (2.79617 and 5.72656 for metal–metal bonding only and all bondings respectively) for Arrangement 1 (TaNbS) are greater than the corresponding ones (2.57451 and 5.63995) for Arrangement 2 (NbTaS). The charges on the metal positions are closer to each other in Arrangement 1 (TaNbS) than in Arrangement 2 (NbTaS). This means that the metal–metal bonding and overall bonding are more effective in Arrangement 1 (TaNbS) than they are in Arrangement 2 (NbTaS). The difference (0.22166) in summation of OP for all metal–metal bonds between the two arrangements is much greater than that (0.08661) for summation of OP for all bonds, *i.e.*

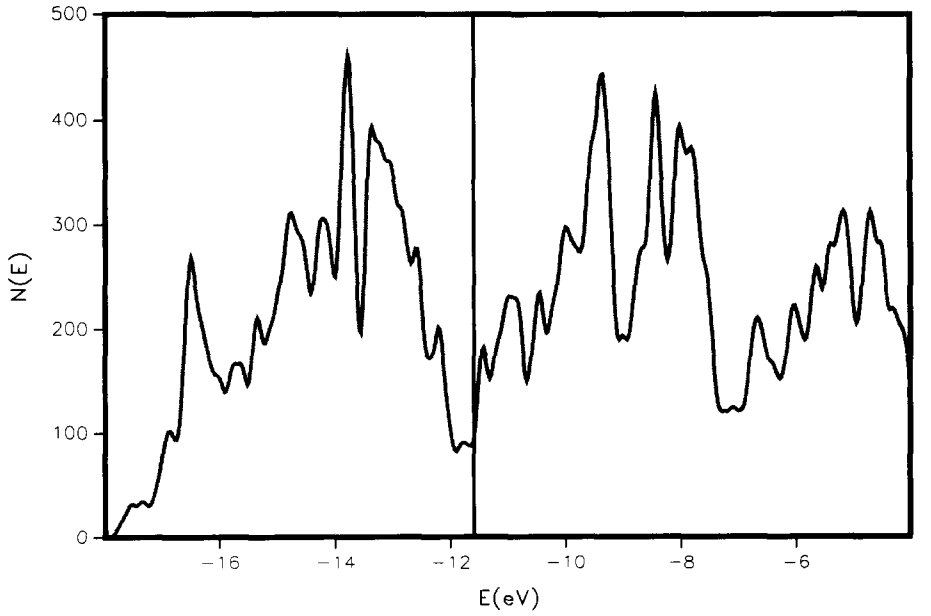

Fig. 3. Total DOS curve of TaNbS. The Fermi level is marked by the vertical line.

TABLE 6

Average energy, Fermi energy and overlap populations (OP) for two arrangements

	Arrangement 1 (TaNbS)	Arrangement 2 (NbTaS)
Average energy (eV)	−486.215	−486.180
Fermi level (eV)	−11.603	−11.670
Overlap population		
M1–M1 (333 pm) (2)[a]	0.17346	0.11336
M1–M1 (282 pm) (2)	0.51574	0.38513
M1–M2 (293 pm) (4)	0.28520	0.29818
M1–M2 (329 pm) (1)	0.16613	0.18757
M1–S (269 pm) (1)	0.42488	0.29101
M2–M2 (333 pm) (2)	0.05542	0.09862
M2–S (254 pm) (4)	0.51506	0.58972
M2–S (312 pm) (1)	0.18847	0.20213
S–S (333 pm) (2)	0.03007	0.01936
S–S (320 pm) (2)	0.09833	0.08735
Summation of OP (M–M)[b]	2.79617	2.57451
Summation of OP[c]	5.72656	5.63995

[a]The number of symmetry-unique bonds in one primitive cell.
[b]The summation of OP for all metal–metal pairs in one primitive cell.
[c]The summation of OP for all pairs of atoms in one primitive cell.

TABLE 7

Charges on each atomic position for two arrangements

Atom	Arrangement 1 (TaNbS)	Arrangement 2 (NbTaS)
M1	5.267	5.572
M2	5.117	4.830
S	5.616	5.597

including metal–metal, metal–sulfur and sulfur–sulfur bonds, between the two arrangements; this means that there is a trade-off of metal–metal bonds for some other bonds in Arrangement 1. Because Arrangement 1 (TaNbS) is closer to that of the real compound, the calculations provide a basis for understanding why Nb preferentially occupies the metal position bound to more coordinating S. The fact that the average energy for Arrangement 1 (−486.215 eV) is slightly lower than that (−486.180 eV) for Arrangement 2 also supports the explanation given above.

The fact that metal–metal bonding is more effective in Arrangement 1 (TaNbS) than in Arrangement 2 (NbTaS) can be understood in terms of relative electronegativities. The electronegativities of Ta, Nb and S are 1.5, 1.6 and 2.5 [17] respectively. The difference in electronegativities between Ta and S (1.0) is greater than that between Nb and S (0.9), *i.e.* Ta would

lose more electron density to S than would Nb, were they equivalently bound to S. Thus, Nb in comparison with Ta is more effective in forming metal–metal bonds when equivalently bound to S. Thus, the structure of Arrangement 1 is favored over that of Arrangement 2 by the enhanced metal–metal bonding of Arrangement 1.

The average energy difference between the two arrangements (0.035 eV) is so small and the reacting temperature (above 2500 K) is so high that entropic stabilization drives fractional occupancy of each metal position, rather than the idealized TaNbS arrangement.

Figure 4 is a plot of averaged crystal orbital overlap population (COOP). A COOP curve provides us with information about the bonding (or antibonding) character of the system's crystal orbitals with respect to any specific symmetry-unique pair of atoms in the structure. There are a large number of unique metal–metal bonds in the structure, yet we are more interested in the overall metal–metal bonding of $Nb_xTa_{2-x}S$. Thus, the COOP curves are averaged over all the short metal–metal bonds in the structure and appropriately weighted to reflect the number of each symmetry-unique bond. The Fermi level lies on the dividing line between the bonding region and the antibonding region, *i.e.* all of the bonding region is occupied and the antibonding region empty; thus, the maximum metal–metal bonding is achieved in $Nb_xTa_{2-x}S$. The formation of maximum metal–metal bonding in the metal-rich compounds was also observed in Ta_6S_n ($n=3$, 4, 5) [18].

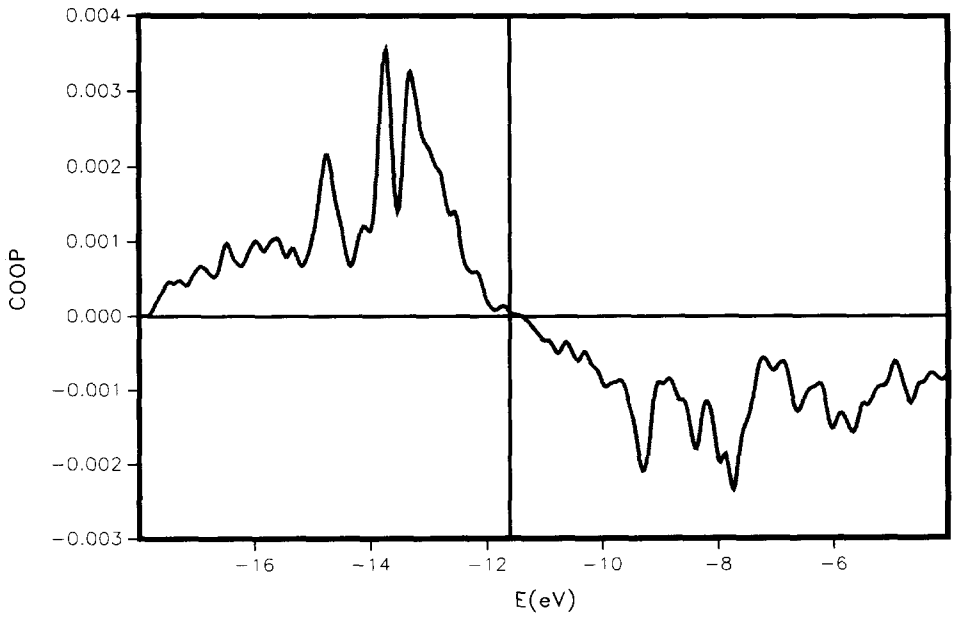

Fig. 4. Averaged metal–metal COOP curve of TaNbS. The Fermi level is marked by the vertical line.

Measurements of electrical properties (superconductivity and electrical conductivity) of $Nb_xTa_{2-x}S$ and $Nb_xTa_{5-x}S_2$ are being carried out by colleagues in the Physics Department at the Iowa State University. $Nb_xTa_{2-x}S$ and $Nb_xTa_{5-x}S_2$ belong to a new class of layered compounds with two characteristics, namely layered compounds with robustly metallic regions separating the van der Waals layers and with a b.c.c. basis. The robustly metallic region between the two settings of van der Waals layers can be easily seen in Fig. 2. Inorganic and organic intercalation studies of layered transition metal disulfides, *e.g.* TiS_2, NbS_2 and MoS_2 (h.c.p. setting) [19], have been of interest for many years and many useful properties have been found. Because there is a vital difference between this new class of the layered compounds and the transition metal disulfides, *i.e.* the previously discussed robustly metallic regions between the two settings of van der Waals layers, it can be expected that some new properties may be found from the organic and inorganic intercalation studies of the two new layered compounds, $Nb_xTa_{2-x}S$ and $Nb_xTa_{5-x}S_2$.

Acknowledgments

We thank Professor R. A. Jacobson and his group for their valuable assistance in the crystallographic portion of the study. We also express our appreciation to Dr. Warren Straszheim for the EDAX analysis. This research was supported by the National Science Foundation, Solid State Chemistry, via grant DMR-8721722 and was carried out in facilities of the Ames Laboratory, Department of Energy, USA.

References

1 B. Harbrecht and H. F. Franzen, *Z. Kristallogr., 186* (1989) 119.
2 H. F. Franzen, T. A. Beineke and B. R. Conard, *Acta Crystallogr. Sect. B, 24* (1968) 412.
3 B. Harbrecht, *Z. Kristallogr., 182* (1988) 118.
4 X. Yao and H. F. Franzen, *J. Less-Common Met., 161* (1990) L37.
5 A. Nyland, *Acta Chem. Scand., 20* (1966) 2393.
6 B. Harbrecht, personal communication, 1989.
7 H.-Y. Chen, R. T. Tuenge and H. F. Franzen, *Inorg. Chem., 12* (1973) 552.
8 B. Harbrecht and H. F. Franzen, *Z. anorg. allg. Chem., 551* (1987) 74.
9 X. Yao and H. F. Franzen, unpublished research, 1989.
10 X. Yao and H. F. Franzen, *J. Solid State Chem., 86* (1990) 88.
11 X. Yao and H. F. Franzen, *Z. anorg. allg. Chem., 598* (1991) 353.
12 X. Yao and H. F. Franzen, *J. Am. Chem. Soc., 113* (1991) 1426.
13 B. Harbrecht, *Angew. Chem., Int. Ed. Engl., 28* (1989) 1660.
14 F. Kadijk and F. Jellinek, *J. Less-Common Met., 19* (1969) 421.
15 N. Walker and D. Stuart, *Acta Crystallogr. Sect. A, 39* (1983) 158.
16 S. Alvares, personal communication, 1984.
17 L. Pauling, *The Chemical Bond*, Cornell University Press, Ithaca, NY, 1967, p. 64.
18 S.-J. Kim, K. S. Nanjundaswamy and T. Hughbanks, *Inorg. Chem., 30* (1991) 159.
19 M. S. Whittingham, *Prog. Solid State Chem., 12* (1978) 41.